ADVANCED MATERIALS INTERFACES
www.advmatinterfaces.de

Stacking Relations and Substrate Interaction of Graphene on Copper Foil

*Philip Schädlich, Florian Speck, Chamseddine Bouhafs, Neeraj Mishra, Stiven Forti, Camilla Coletti, and Thomas Seyller**

The crystallinity of graphene flakes and their orientation with respect to the Cu(111) substrate are investigated by means of low-energy electron microscopy (LEEM). The interplay between graphene and the metal substrate during chemical vapor deposition (CVD) introduces a restructuring of the metal surface into surface facets, which undergo a step bunching process during the growth of additional layers. Moreover, the surface facets introduce strain between the successively nucleated layers that follow the topography in a carpet-like fashion. The strain leads to dislocations in between domains of relaxed Bernal stacking. After the transfer onto an epitaxial buffer layer, the imprinted rippled structure of even monolayer graphene as well as the stacking dislocations are preserved. A similar behavior might also be expected for other CVD grown 2D materials such as hexagonal boron nitride or transition metal dichalcogenides, where stacking relations after transfer on a target substrate or heterostructure could become important in future experiments.

1. Introduction

Although graphene research started with samples obtained by mechanical exfoliation of thin flakes from highly oriented pyrolytic graphite,[1] graphene synthesis for technological purposes requires a scalable low-cost routine. Besides the sublimation growth from a SiC surface,[2,3] one promising candidate for graphene production is chemical vapor deposition (CVD) on metal substrates because it is reproducible, scalable, and leads to high-quality layers with large domain size. Various transition metals have been tested as substrates so far[4–10] of which copper foils have proven to be a suitable substrate for controlled monolayer and bilayer growth due to the low carbon solubility.[11–14] Typically, nucleation of graphene domains on copper foil happens with random orientation, leading to polycrystalline monolayer graphene sheets[15] and even twisted bilayer graphene.[16] Upon coalescence of adjacent domains, grain boundaries are introduced, which limit the carrier mobility.[17] Using the hexagonal Cu(111) surface as a substrate, it was shown that graphene nucleation occurs in registry with the substrate lattice, thus effectively reducing grain boundaries.[18,19] For applications it is necessary to transfer the graphene from the metal substrate to a nonmetallic target substrate (e.g., SiO_2, SiC). In many cases, the quality of the transferred layers lags behind the as-grown graphene. It is well known that the choice of substrate might influence the graphene properties.[20–22] On the one hand, Kraus et al. suggested earlier that facets of the copper substrate might be imprinted in the graphene leading to rippled layers after transfer even on a flat substrate.[23] On the other hand, it was shown that nanoripples in transferred single crystal graphene on SiO_2 degrade the electron mobility.[24] Additionally, in Bernal stacked bilayer graphene, strain induced dislocation lines have been observed on different substrates,[25–27] which potentially limit the carrier mobility. These dislocations could possibly be present even after the transfer on a target substrate. Understanding the formation of these dislocations and the influence of the growth substrate would open a route for engineering the properties of bilayer graphene and other stacked 2D materials.

We utilize low-energy electron microscopy (LEEM) and diffraction (LEED) to investigate the thickness and crystallinity of CVD grown graphene on the Cu(111) substrate and after transfer on an epitaxial buffer layer. We show that the substrate surface undergoes a restructuring into facets upon graphene growth, which imprint a rippled structure even in monolayer graphene. LEEM dark-field measurements reveal the role of the substrate facets in the formation of stacking domains in bilayer (and trilayer) graphene that are preserved during transfer.

P. Schädlich, Dr. F. Speck, Prof. T. Seyller
Institut für Physik
Technische Universität Chemnitz
Reichenhainer Str. 70, 09126 Chemnitz, Germany
E-mail: thomas.seyller@physik.tu-chemnitz.de

P. Schädlich, Dr. F. Speck, Prof. T. Seyller
Center for Materials
Architectures and Integration of Nanomembranes (MAIN)
Rosenbergstr. 6, 09126 Chemnitz, Germany

Dr. C. Bouhafs, Dr. N. Mishra, Dr. S. Forti, Dr. C. Coletti
Center for Nanotechnology Innovation@NEST
Istituto Italiano di Tecnologia
Piazza San Silvestro 12, Pisa 56127, Italy

Dr. C. Bouhafs, Dr. N. Mishra, Dr. C. Coletti
Graphene Labs
Istituto Italiano di Tecnologia
Via Morego 10, Genova 16163, Italy

The ORCID identification number(s) for the author(s) of this article can be found under https://doi.org/10.1002/admi.202002025.

© 2021 The Authors. Advanced Materials Interfaces published by Wiley-VCH GmbH. This is an open access article under the terms of the Creative Commons Attribution License, which permits use, distribution and reproduction in any medium, provided the original work is properly cited.

DOI: 10.1002/admi.202002025

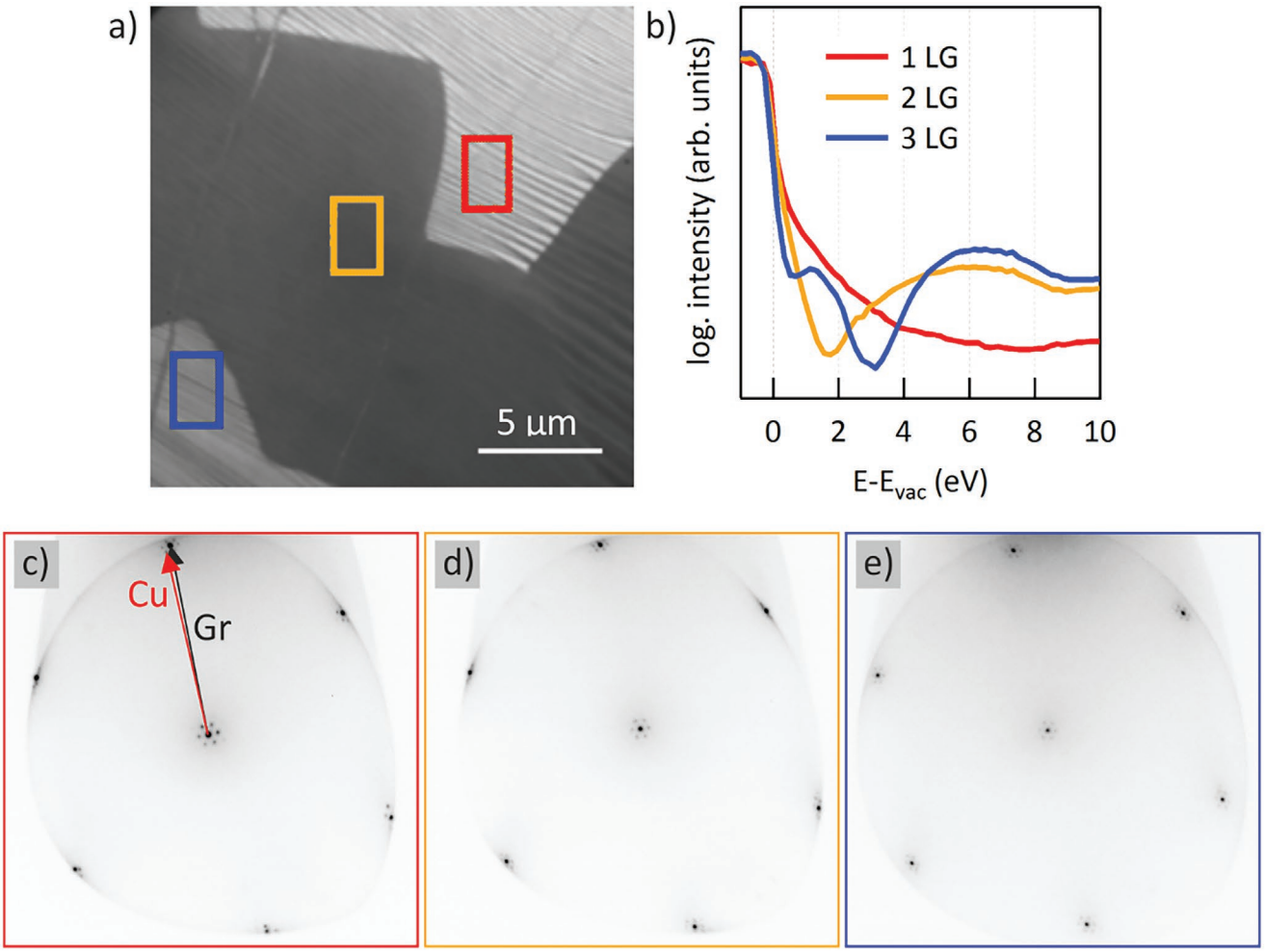

Figure 1. a) LEEM bright-field image (E = 2.2 eV) of CVD grown graphene on Cu(111). A pattern of dark stripes is observed on the graphene covered surface, which signals a restructuring of the substrate surface into facets. b) LEEM reflectivity spectra of the individual areas marked in the image allow the identification of the local coverage of the substrate with graphene. c–e) Selected area LEED measurements from areas with increasing coverage (1 LG, 2 LG, and 3 LG) marked in (a). The arrows in (c) indicate the reciprocal lattice vectors of graphene (Gr) and the Cu(111) surface (Cu).

2. Graphene on Cu(111)

During the CVD process, graphene growth starts at multiple nucleation points, which appear as the center of concentric bi- and multilayer domains with size up to several hundreds of micrometers. These bi- and multilayer domains are surrounded by homogeneous monolayer graphene covering the space between the domains. An overview photoemission electron microscopy (PEEM) image of the sample is given in Figure S1a in the Supporting Information. **Figure 1a** shows a LEEM image from the corner of an as-grown graphene sheet with monolayer graphene (1 LG) in the top right and increasing coverage (2 LG and 3 LG) toward the bottom left. The local coverage is determined by low-energy electron reflectivity spectra (also termed LEEM I–V spectra). Figure 1b shows typical spectra for one to three layers of graphene. The number of minima in the reflectivity curves is related to the number of graphene layers and associated interlayer states.[28,29] For 1 LG, one broad minimum is obtained at roughly 8 eV corresponding to the interlayer state between the graphene layer and the Cu(111) surface.[30] For 2 LG and 3 LG, we find one (1.7 eV) and two additional minima (0.6 and 3.0 eV) according to the graphene interlayer states, respectively.[28,29] The energy scale of the spectra is normalized with respect to the vacuum energy E_{vac}, which is determined from the mirror mode transition by the method described in ref. [30]. The mirror mode transition is the electron energy at which the majority of electrons overcome the sample potential and interact with the surface, leading to a rapid decrease of the reflected intensity.

Figure 1c–e shows selected area LEED measurements on areas with increasing coverage, i.e., on the domain structures, with the same sixfold diffraction pattern independent on the coverage. From this we find that all layers nucleate with the same rotational alignment (Bernal stacked). The arrows in Figure 1c indicate the reciprocal lattice vectors of the graphene (Gr) and the Cu(111) surface (Cu), respectively. The slight mismatch between the two lattices leads to moiré spots surrounding the specular diffraction spot and the first order diffraction spots, which will be discussed later. At this point, we

© 2021 The Authors. Advanced Materials Interfaces published by Wiley-VCH GmbH

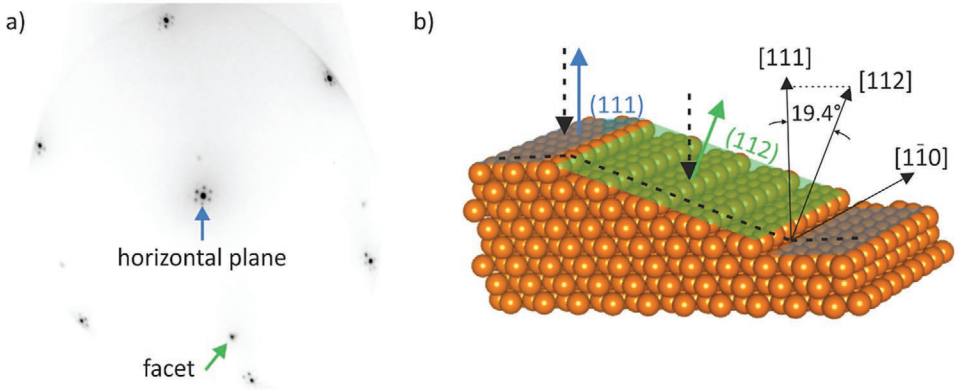

Figure 2. a) LEED pattern (E = 50 eV) showing two sets of diffraction spot due to graphene on inclined planes. The (00) spot of each pattern is indicated as "horizontal plane" and "facet," respectively. b) The sketch illustrates the scattering geometry for horizontal (111) planes (blue) to which the microscope is aligned and for inclined (112) planes (green) for the same incoming electron beam (black, dashed). From the spot movement ("facet") in reciprocal space for increasing energy, an inclination angle of (19 ± 1)° is determined (see the Supporting Information).

want to mention that the intensity of these satellite diffraction spots decreases for LEED patterns obtained from areas with increasing graphene coverage because the contribution from the buried substrate gets weaker.

2.1. Faceting of the Cu Surface

The pattern of dark stripes in the 1 LG area in Figure 1 arises due to inclined surface planes. A similar behavior was observed before for graphene on Cu(100).[16,23] **Figure 2a** shows a LEED image of such a monolayer region. The sixfold diffraction pattern of graphene on Cu(111) and the typical moiré spots surrounding the first order diffraction spots as well as the specular reflection (marked by "horizontal plane") in the center are clearly visible. In addition, a displaced set of diffraction spots with the (00) spot marked as "facet" in Figure 2a is observed. The displacement of the specular reflection of this facet with respect to that of the flat (111) area ("horizontal plane") is caused by an inclination, which is further investigated below. This facet appears dark in the LEEM bright-field (BF) image because electrons impinging the surface normal to the (111) direction are not reflected parallel to the optical axis of the microscope as indicated in Figure 2b. The microscope is aligned to the horizontal (111) surface planes, which lead to the graphene diffraction spots that are concentrically distributed around the (00) spot marked as "horizontal plane." Obviously, the specular diffraction spot of the inclined plane is shifted perpendicular to the [1$\bar{1}$0] direction with respect to the centered diffraction pattern. From this, we conclude that the step edges of the surface facets run along the [1$\bar{1}$0] direction or the zigzag edge of the graphene sheet, respectively.

An identification of the tilt angle between the (111) surface ("horizontal plane") and the inclined facets ("facet") is possible by observing the energy-dependent position of its specular diffraction spot. Using the method introduced by Tang et al., we determined a tilt angle of (19 ± 1)° (see also the Supporting Information).[31] Based on this value and on the orientation of the facets along the [1$\bar{1}$0] direction, we therefore suggest that the Cu(111) surface undergoes a restructuring into (111) and (112) planes.

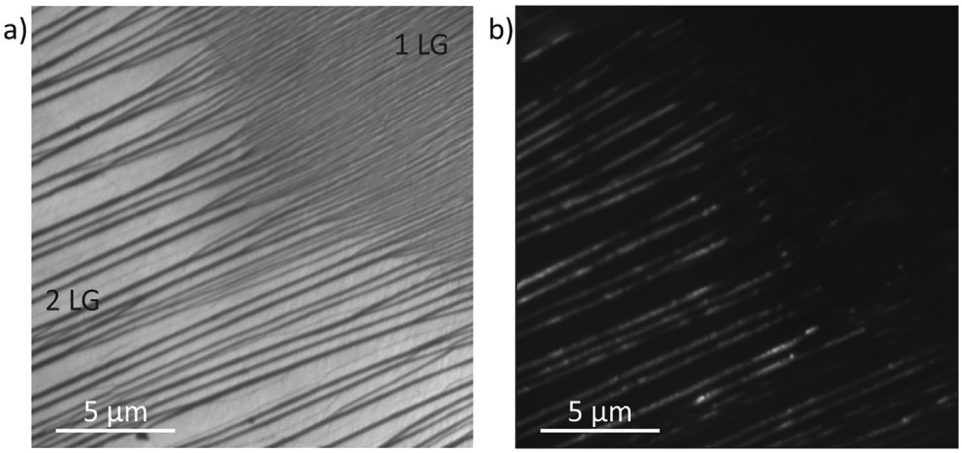

Figure 3. a) The LEEM bright-field image using the (00) spot marked as "horizontal plane" in Figure 2a from the corner of a graphene domain shows the stripe pattern due to the surface facets. The local coverage of 1 LG and 2 LG is known from reflectivity data. b) In the dark-field image using the (00) spot of the inclined planes ("facet" in Figure 2a), the contrast is inverted.

© 2021 The Authors. Advanced Materials Interfaces published by Wiley-VCH GmbH

Figure 3 compares a LEEM-BF image obtained by using the specular reflection of the flat (111) surface (Figure 3a) with a LEEM dark-field image obtained with the help of the (00) spot of the inclined facets (Figure 3b). While the inclined facets appear dark in the former image, they appear bright in the latter one. Obviously, the stripe pattern is inverted. This confirms the restructuring into large (111) areas and tilted (112) facets. A similar stripe pattern was observed by optical microscopy in ref. [37] for graphene multilayers on copper substrates, which only appeared in areas covered by graphene. Interestingly, the density of stripes observed here differs between 1 LG and 2 LG areas, where the number of stripes and thus number of facets per unit length is lower by a factor of ≈3. This indicates a step-bunching like process during the growth of the second graphene layer such that adjacent (111) terraces merge together. This might point toward a strong C–Cu interaction that influences the process of reshaping the copper surface during growth.

The diffraction patterns (such as Figure 2a) also show that the (00) spot of the graphene covered (111) planes is surrounded by six additional satellite spots. Those satellite spots arise due to multiple scattering from the graphene and the copper lattice, respectively.[19] The position of the spots corresponds to the scattered electron's wave vector parallel to the surface

$$\vec{k}_{\parallel,\mathrm{out}} = \vec{k}_{\parallel,\mathrm{in}} + \vec{G}_{\mathrm{gr}} - \vec{G}_{\mathrm{Cu(111)}} \tag{1}$$

where $\vec{k}_{\parallel,\mathrm{out}}$ and $\vec{k}_{\parallel,\mathrm{in}}$ are the in-plane components of the wave vector of the scattered and incident electrons, and $\vec{G}_{\mathrm{gr}}$ and $\vec{G}_{\mathrm{Cu(111)}}$ are the 2D reciprocal lattice vectors of graphene and the Cu(111) surface, respectively. Robinson et al. found that for graphene in rotational alignment with the Cu(111) lattice, the superstructure spots are aligned with the first order spots too.[19] Interestingly, the orientation of the satellite spots in Figure 2a differs from the orientation of the graphene first order spots. In **Figure 4a**, the magnified LEED pattern from a single domain of graphene on Cu(111) shows a 30° rotation between the satellite spots and the graphene spots. With the help of a simple model where we calculate the position of the double-diffraction spots for various rotation angles between the graphene (black dots) and Cu(111) (orange dots) reciprocal lattice, we are able to reproduce the orientation of the satellite spots (blue dots) in Figure 4a. The inset shows the result for a 1° rotation between the two lattices, which indeed results in a 30° rotation of the double-diffraction spots. Therefore, the orientation is very sensitive to the graphene–Cu(111) alignment. In the magnified LEED pattern of a different domain in Figure 4b, the graphene and the satellite spots are equally oriented and the inset shows that this is a consequence of a perfect alignment of the graphene with respect to the substrate.[19] With the help of this model, we find that the sample shows a maximum rotation between graphene and Cu(111) of ±1° except for rare cases close to larger defect structures.

2.2. Identification of Stacking Domains

Figure 5a shows a LEEM bright-field image of a homogeneous bilayer area with the alternating sequence of horizontal Cu(111) and inclined Cu(112) surface planes. The image is taken with the (00) spot of the horizontal areas as it is indicated in the inset. In contrast, the dark-field image of that area (see Figure 5b) using a first order diffraction spot of graphene reveals a surface composed of two domains of different contrast. The size and shape of these domains is similar to the facet induced stripe pattern in the bright-field image. Comparable domains in bilayer graphene have been observed on copper[25,26] and SiC[27] and were attributed to the strain induced formation of dislocation lines. In the dislocation line, a lateral shift of one C—C bond length between the two layers is realized, thus leading to relaxed Bernal stacking configurations (AB and AC) in between. The inset in Figure 5b illustrates the stacking configuration for AB and AC stacked bilayer graphene. LEED *I–V* curves were measured by recording the energy-dependent reflectivity in dark-field geometry. The spectra obtained from the blue and the orange

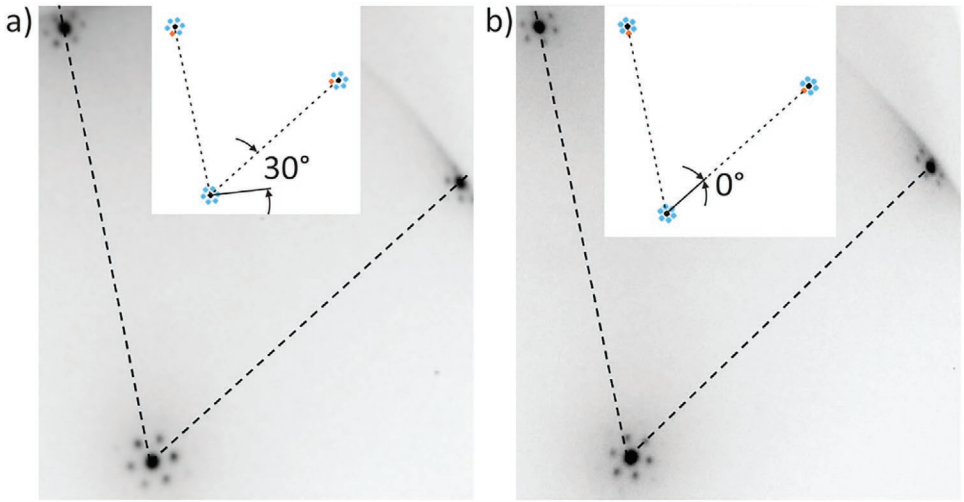

Figure 4. Magnified LEED images (E = 50 eV) show satellite spots due to multiple scattering from the graphene and the Cu(111) surface. Depending on the orientation between the graphene and copper lattice, the superstructure spots are a) rotated or b) aligned to the first order diffraction spots.

© 2021 The Authors. Advanced Materials Interfaces published by Wiley-VCH GmbH

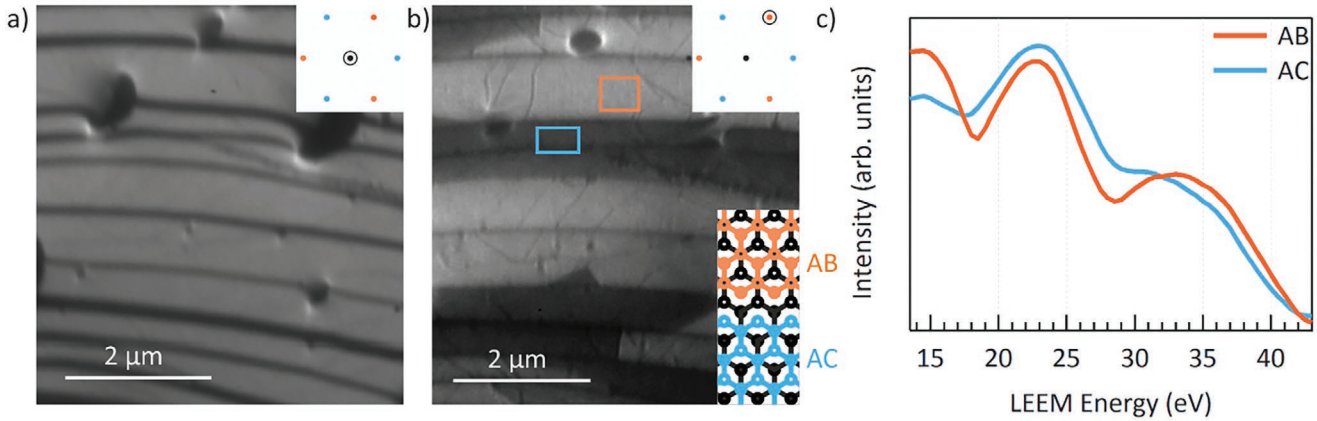

Figure 5. a) LEEM bright-field measurement ($E = 11$ eV) from an area with homogeneous bilayer coverage. Bright and dark stripes are due to horizontal and inclined surface planes. b) LEEM dark-field image ($E = 37$ eV) from the area in (a). Domains of alternating contrast become visible while the contrast changes occur close to the inclined (112) planes (compare with (a)). The inset illustrates the difference between the AB and AC Bernal stacking configuration. c) LEED *I–V* spectra measured in the marked areas corresponding to AB and AC Bernal stacking domains.

box on two different types of domains are shown in Figure 5c. While the different domains show the same bright-field reflectivity (due to the same coverage), the LEED *I–V* spectra are clearly distinguishable. Furthermore, the spectra are in excellent agreement with the results of de Jong et al. for AB and AC stacked bilayer graphene on SiC.[27] From this, we can conclude that the bright areas in Figure 5b are AB stacked and the darker areas in Figure 5b are AC stacked bilayer graphene.

It was shown by de Jong et al. that uniform strain leads to triangular shaped domains while elongated domains are the result of anisotropic strain,[27] which obviously is the case here. From Figure 5a,b, we find that the contrast inversions in the dark-field image, i.e., the dislocation lines, occur in the vicinity of boundaries between (111) and (112) planes of the Cu surface. Considering a model in which the graphene layers cover the surface in a carpet-like manner with otherwise constant structural parameters (interatomic distances and layer distances) would not result in the observation of different stacking on the (111) areas of the surface. On the other hand it is plausible to assume that the graphene–substrate interaction differs for Cu(111) and Cu(112). The latter surface is much more open and shows a stronger corrugation of the surface.[32] In addition, the (112) surface has not the same symmetry as the (111) surface (see **Figure 6**). While the latter has sixfold rotational symmetry (threefold if the bulk stacking is taken into account), the (112) surface has only a mirror symmetry with a mirror plane perpendicular to the step edges. It is therefore reasonable to assume that the graphene–substrate interaction on the (112) oriented areas of the surface induces uniaxial strain in the bottom graphene layer of the bilayer stack. From the LEEM image in Figure 5a, we determine a width of ≈0.1 to 0.2 µm of the (112) facets, which corresponds to $\approx 10^3$ lattice constants. A switch from AB to AC stacking requires a shift of 0.14 nm (C—C bond length) in a direction perpendicular to the zigzag direction of one of the layers over the width of the (112) facet. This corresponds to a strain of the order of 0.1%, which is not unlikely in graphene on metal surfaces. As stated above, the steps of the (112) facets run parallel to the zigzag direction of graphene, which fits to the shift necessary for the AB/AC transition. The restructuring of the substrate surface during the growth process thus enforces the formation of differently stacked domains and might therefore degrade the electronic properties of the grown layers.

3. Transfer on Epitaxial Buffer Layer

In order to characterize the influence of the substrate-induced inhomogeneity on the system after transfer to a target substrate, we investigate the CVD grown layers after transfer on

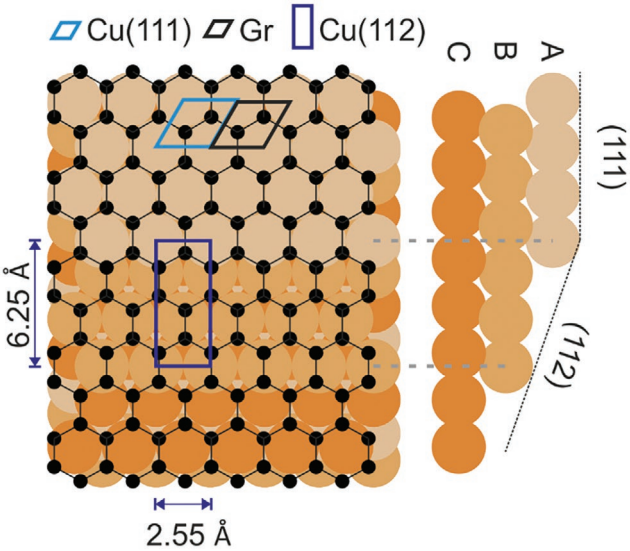

Figure 6. Schematic of the facetted copper surface with one graphene layer on top in top view and side view. Equally colored copper atoms are in the same (111) plane. For clarity, only one graphene layer is shown. On the (112) planes, a lattice mismatch between the Cu lattice and the graphene lattice is introduced. In the side view, the layer sequence of Cu(111) planes is indicated (ABC). The unit cell of the Cu(111), Cu(112), and the graphene (Gr) lattice is shown in the image.

© 2021 The Authors. Advanced Materials Interfaces published by Wiley-VCH GmbH

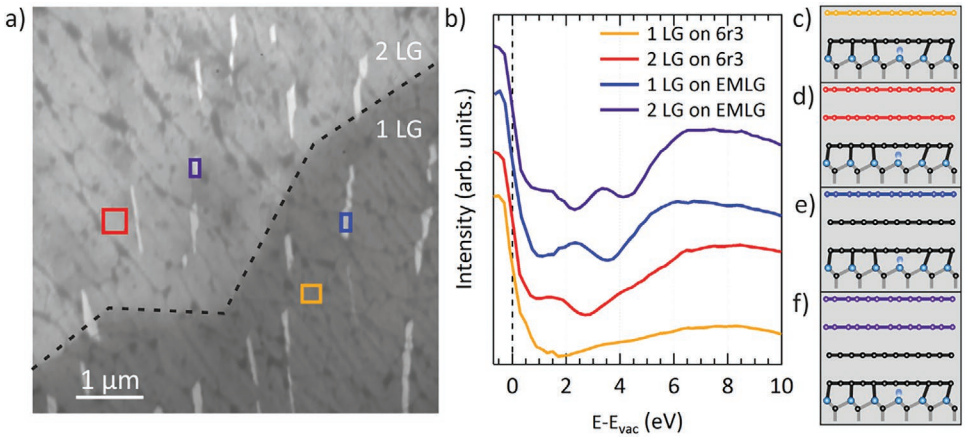

Figure 7. a) LEEM bright-field image (E = 11.4 eV) of 1 LG (bottom) and 2 LG (top) after the transfer onto an epitaxial buffer layer (6r3). Reflectivity spectra are recorded in the marked areas and shown in (b). c–f) Sketch of the local coverage of 1 LG on the 6r3, 2 LG on 6r3, 1 LG on epitaxial monolayer graphene (EMLG), and 2 LG on EMLG, respectively. Here, substrate carbon atoms are black and silicon atoms are blue while transferred graphene layers are color-coded as in the respective area and reflectivity spectrum.

an epitaxial buffer layer on SiC(0001). An overview PEEM image of the sample after the transfer is given in Figure S1b in the Supporting Information. **Figure 7a** shows a bright-field LEEM image from the corner of a graphene domain on the buffer layer. The image consists of mainly two areas with different reflectivity separated by a boundary running more or less diagonally from the lower left side to the upper right side. This is due to a different thickness of the CVD graphene transferred as indicated in Figure 7a. In addition, bright patches elongated in vertical direction can be observed. These correspond to partial epitaxial monolayer graphene (EMLG) that nucleates along the SiC step edges.[3] From this observation, we can derive the important information that SiC step edges run in vertical direction in Figure 7a. Next, we observe a pattern of thin dark lines running diagonally from the top left to the bottom right in Figure 7a. This pattern shows strong similarities with the pattern of (111) and (112) facets on the copper surface. Both size and shape of the structures are very similar and LEED showed that the direction of the thin dark lines corresponds to the zigzag direction of graphene as discussed above. From these observations, we conclude that structural imperfections caused by faceting of the Cu surface are indeed imprinted into the CVD grown graphene and are preserved during transfer. Previously, Kraus et al. suggested that the presence of the substrate facets imprinted into the graphene would prevent the layers from being flat after the transfer onto a flat target substrate[23] leading to a periodically rippled surface with limited carrier mobility.[24]

Figure 7b depicts LEEM I–V curves of the different areas marked in Figure 7a by differently colored rectangles. As discussed in the following, the spectra can be used to determine the local structure. The different layer sequences in the respective areas are sketched in Figure 7c–f for clarity. The LEEM I–V curve from 1 LG on 6r3 (yellow) shows one minimum as it is expected for monolayer graphene on SiC.[28,33] However, the reflectivity minimum appears rather flat compared to epitaxial monolayer graphene.[34] This could be due to a locally varying distance between the buffer layer and the transferred layer, which is introduced by the imprinted facets, because the position of the reflectivity minimum is highly sensitive to the separation.[29] Please note that adsorbates present on the buffer layer could also influence the graphene–buffer layer distance and the minimum's energy position. Another point that has to be considered is the rotational alignment between the buffer layer and the transferred layers that might differ from epitaxial graphene. For example, from µ-LEED measurements in the discussed area, we find a rotation of (13 ± 1)° between the buffer layer and graphene lattice of the transferred layers. However, to our knowledge, the effect of the rotational misalignment on the energy position of reflectivity minima has not been investigated so far. For 2 LG on 6r3 (red), we find two minima in the spectrum as expected for epitaxial bilayer graphene on SiC.[28] On the EMLG patches, the local coverage is increased by one graphene layer and therefore it is not surprising that we observe two minima centered at about 2 eV for 1 LG on EMLG (blue). Obviously, the spectrum shows a similar number of dips as for 2 LG on 6r3 but here both minima are well pronounced, thus, pointing toward a cleaner interface between the EMLG and the transferred layer. In analogy, for 2 LG on EMLG, we find three dips in the I–V curve, of which the low energy dip appears only as a shoulder close to the mirror mode transition. As it would be expected for epitaxial graphene, the three dips are also centered at roughly 2 eV, which indicates a symmetric splitting of the interlayer states.[35] Thus, on the EMLG patches, we find an interface between the substrate and the transferred layers that is close to what we find for epitaxial graphene on SiC while the interface on the buffer layer is probably affected by adsorbates and a locally varying separation. The influence of the ripples on the local separation between the EMLG and the transferred layers is difficult to address because the EMLG patches are rather small. Nevertheless, it is worth thinking about the EMLG as a more suitable substrate for further transfer experiments because it exhibits a cleaner interface.

Now, we want to address the question: how are the stacking domains affected by the transfer? **Figure 8a** shows a bright-field image of the transferred graphene layers, where the local coverage of 2 LG and 3 LG is determined from the reflectivity spectra as it is illustrated in the inset. The dark-field image (see

© 2021 The Authors. Advanced Materials Interfaces published by Wiley-VCH GmbH

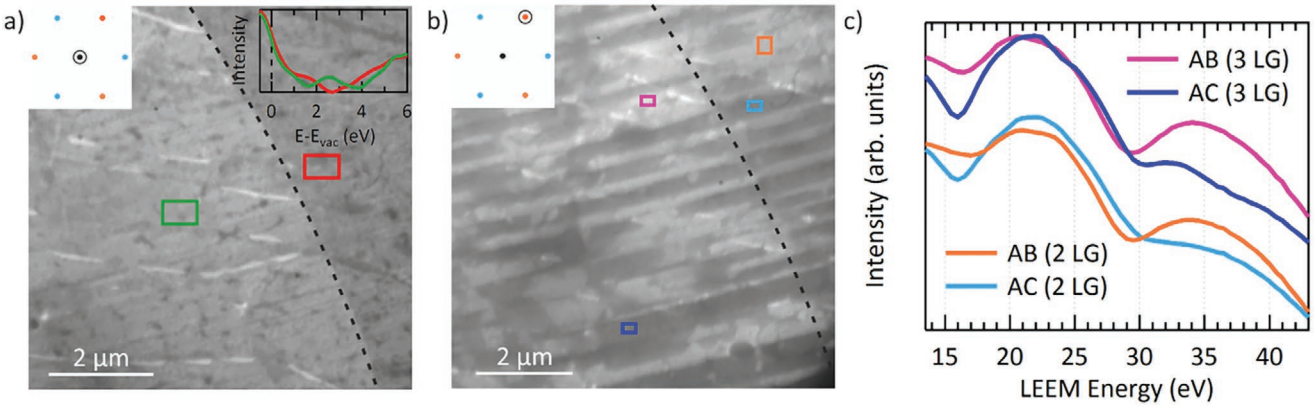

Figure 8. a) Bright-field image (E = 2.3 eV) of a graphene flake transferred on a buffer layer. The local coverage of 2 LG and 3 LG was inferred from I–V spectra from the marked areas as indicated in the inset. b) Dark-field image (E = 34 eV) of the position in (a), where a first order spot of graphene is used for imaging. Domains of alternating contrast become visible in the 2 LG as well as in the 3 LG area. The comparison with (a) shows that the contrast switches along the line pattern induced by the faceting of the former substrate. c) The LEED I–V spectra measured in the marked areas for 2 LG (orange, light blue) and 3 LG (pink, blue) correspond to AB and AC stacking between the top-most graphene layers, respectively.

Figure 8b), which was obtained with the indicated first order diffraction spot shows domains of alternating contrast as it was observed on the copper foil. From the comparison with the bright-field image in Figure 8a, it gets clear that the domain boundaries caused by the facets of the copper substrate run along the dark lines in the bright-field image. The LEED I–V spectra measured from a dark and a bright domain on the 2 LG and 3 LG area, respectively, are shown in Figure 8c. The orange and the light blue spectrum obtained from the bilayer region are indeed very similar to what we have measured for AB and AC stacked bilayer areas on the copper foil (see Figure 5c). In addition, we find comparable spectra on the 3 LG area (pink and blue). Here, the stacking configuration for three layers can be ABA, ABC, ACA, or ACB. Due to the low information depth of electrons in that energy range, the first two and the latter two fall into two groups named AB or AC, respectively (see also Figure 7c).[27] An unambiguous differentiation between the two members of each group was not possible in our experiment. The observation of the domain structure consisting of differently stacked bilayer and trilayer graphene in layers transferred on the epitaxial buffer layer clearly demonstrates that these structural imperfections, which are caused by the facetted nature of the Cu substrate, are robust enough to survive the transfer process.

4. Conclusion

In summary, we have used LEEM and µ-LEED to study the structure of graphene on a Cu(111) substrate directly after CVD and after transfer on an epitaxial buffer layer on SiC. In general, the orientation of the graphene layers and the Cu(111) surface was observed to be aligned within ± 1° and no rotational disorder was observed for multilayers. A restructuring of the substrate into wider (111) oriented planes and narrower (112) oriented facets was observed, which occurs during growth. The boundaries between the two different orientations give rise to stacking domain boundaries in bilayer and trilayer graphene. We propose that the latter are the result of an uniaxial strain caused by the interaction of the graphene layers with the (112) facets. After transfer, identical structures are observed, which demonstrates the stability of the structural imperfections imprinted by the facet structure of the substrate. We expect that the imprinted structure leads to small distance variations between the target substrate and the transferred layers leading to a rippled structure. Indirect evidence for this is provided by the large width of the reflectivity minimum observed for 1 LG transferred on the epitaxial buffer layer. Distance variations between the graphene layers and the target substrate might deteriorate the transport properties due to, e.g., inhomogeneous doping. Second, the dislocation network could have a negative impact on the electronic transport in the transferred bilayer graphene as well. It is worth mentioning that a similar behavior might also be expected for other 2D materials such as hexagonal boron nitride or transition metal dichalcogenides grown by CVD on metallic substrates.

5. Experimental Section

Sample Preparation: Graphene was grown using a 4 in. Aixtron BM-Pro cold-wall reactor. An electropolished 25 µm thick Cu foil (Alfa-Aesar #46365, 99.8% purity) was used as a substrate and the effective gas flow was reduced by means of a sample enclosure.[36] Specifically, growth was implemented on a Cu foil suspended over two Cu supports (about 100 µm thick) placed on top of the graphite susceptor.[37] The growth process consisted of four steps: i) temperature ramp-up, during which the furnace temperature was increased up to a value of 1070 °C (calibrated according to the melting point of Cu) under Ar atmosphere; ii) annealing step carried out at 1070 °C for 10 min under Ar flow; iii) growth step, during which H_2 and CH_4 gases (99.99% purity) were introduced in the growth chamber while keeping the temperature at (1070 ± 1) °C for 90 min (flow rates were set to 100, 1.1, and 900 sccm, for H_2, CH_4, and Ar, respectively); iv) cool-down step performed in Ar and H_2 atmosphere. During the whole process, the pressure was maintained at 25 mbar.

Transfer: Transfer of graphene layers was achieved via standard wet transfer technique using ammonium persulphate solution (APS). Before transfer, the sample was cleaned with isopropanol (IPA) for a few minutes and dried. PMMA was spin-deposited on the sample and baked at 90 °C for 1 min over a hot plate. Since graphene was obtained on both copper sides, the unwanted graphene on the back side was removed by

© 2021 The Authors. Advanced Materials Interfaces published by Wiley-VCH GmbH

reactive ion exchange (RIE) for 1 min in the atmosphere of Ar and O_2. After this step, the copper was etched overnight in a 0.1 M solution of APS. The floating graphene membrane was subsequently rinsed several times with deionized water and transferred on buffer layer graphene on SiC(0001). The sample was kept for 2 h at room temperature to dry and then at 150 °C for 3 h to improve the adhesion of graphene on the substrate. Finally, the sample was cooled down and kept in acetone for 2 h to remove the PMMA and subsequently rinsed in IPA.

Low-Energy Electron Microscopy: LEEM measurements were performed using an FE-LEEM P90 (Specs). The diffraction spots for dark-field imaging were selected by means of an aperture in the back focal plane of the objective lens. By illuminating the sample with a Hg lamp, PEEM images were also collected.

Supporting Information

Supporting Information is available from the Wiley Online Library or from the author.

Acknowledgements

The research leading to these results received funding from the European Union's Horizon 2020 research and innovation program under grant agreement nos. 785219-GrapheneCore2 and 881603-GrapheneCore3.

Open access funding enabled and organized by Projekt DEAL.

Conflict of Interest

The authors declare no conflict of interest.

Data Availability Statement

Research data are not shared.

Keywords

chemical vapor deposition, epitaxial graphene, low-energy electron diffraction, low-energy electron microscopy

Received: November 19, 2020
Revised: January 20, 2021
Published online: February 22, 2021

[1] K. S. Novoselov, A. K. Geim, S. V. Morozov, D. Jiang, Y. Zhang, S. V. Dubonos, I. V. Grigorieva, A. A. Firsov, *Science* **2004**, *306*, 666.
[2] C. Berger, Z. Song, T. Li, X. Li, A. Y. Ogbazghi, R. Feng, Z. Dai, N. Alexei, M. E. H. Conrad, P. N. First, W. A. De Heer, *J. Phys. Chem. B* **2004**, *108*, 19912.
[3] K. V. Emtsev, A. Bostwick, K. Horn, J. Jobst, G. L. Kellogg, L. Ley, J. L. McChesney, T. Ohta, S. A. Reshanov, J. Röhrl, E. Rotenberg, A. K. Schmid, D. Waldmann, H. B. Weber, T. Seyller, *Nat. Mater.* **2009**, *8*, 203.
[4] J. Coraux, A. T. N'Diaye, C. Busse, T. Michely, *Nano Lett.* **2008**, *8*, 565.
[5] T. M. Graphene, B. Wang, M. Caffio, C. Bromley, H. Fru, R. Schaub, *ACS Nano* **2010**, *4*, 5773.
[6] E. Miniussi, M. Pozzo, A. Baraldi, E. Vesselli, R. R. Zhan, G. Comelli, T. O. Menteş, M. A. Niño, A. Locatelli, S. Lizzit, D. Alfè, *Phys. Rev. Lett.* **2011**, *106*, 2.
[7] S. Marchini, S. Günther, J. Wintterlin, *Phys. Rev. B: Condens. Matter Mater. Phys.* **2007**, *76*, 075429.
[8] Y. Yao, Z. Li, Z. Lin, K. S. Moon, J. Agar, C. Wong, *J. Phys. Chem. C* **2011**, *115*, 5232.
[9] J. Wintterlin, M. L. Bocquet, *Surf. Sci.* **2009**, *603*, 1841.
[10] P. W. Sutter, J. Flege, E. A. Sutter, *Nat. Mater.* **2008**, *7*, 406.
[11] X. Li, W. Cai, J. An, S. Kim, J. Nah, D. Yang, *Science* **2009**, *324*, 1312.
[12] X. Li, C. W. Magnuson, A. Venugopal, R. M. Tromp, J. B. Hannon, E. M. Vogel, L. Colombo, R. S. Ruoff, *J. Am. Chem. Soc.* **2011**, *133*, 2816.
[13] W. Wu, Q. Yu, P. Peng, Z. Liu, J. Bao, S. S. Pei, *Nanotechnology* **2012**, *23*, 035603.
[14] S. Bae, H. Kim, Y. Lee, X. Xu, J. S. Park, Y. Zheng, J. Balakrishnan, T. Lei, H. Ri Kim, Y. Il Song, Y. J. Kim, K. S. Kim, B. Özyilmaz, J. H. Ahn, B. H. Hong, S. Iijima, *Nat. Nanotechnol.* **2010**, *5*, 574.
[15] K. Kim, Z. Lee, W. Regan, C. Kisielowski, M. F. Crommie, A. Zettl, *ACS Nano* **2011**, *5*, 2142.
[16] S. Nie, W. Wu, S. Xing, Q. Yu, J. Bao, S. S. Pei, K. F. McCarty, *New J. Phys.* **2012**, *14*, 093028.
[17] X. Fan, S. Wagner, P. Schädlich, F. Speck, S. Kataria, T. Haraldsson, T. Seyller, M. C. Lemme, F. Niklaus, *Sci. Adv.* **2018**, *4*, eaar5170.
[18] S. Nie, J. M. Wofford, N. C. Bartelt, O. D. Dubon, K. F. McCarty, *Phys. Rev. B: Condens. Matter Mater. Phys.* **2011**, *84*, 155425.
[19] Z. R. Robinson, P. Tyagi, T. R. Mowll, C. A. Ventrice, J. B. Hannon, *Phys. Rev. B: Condens. Matter Mater. Phys.* **2012**, *86*, 235413.
[20] J. Ristein, S. Mammadov, T. Seyller, *Phys. Rev. Lett.* **2012**, *108*, 246104.
[21] A. Sinterhauf, G. A. Traeger, D. Momeni Pakdehi, P. Schädlich, P. Willke, F. Speck, T. Seyller, C. Tegenkamp, K. Pierz, H. W. Schumacher, M. Wenderoth, *Nat. Commun.* **2020**, *11*, 555.
[22] P. A. Thiel, L. Huang, A. K. Engstfeld, R. J. Behm, K.-M. Ho, C.-Z. Wang, J. W. Evans, X. Liu, M. C. Tringides, Y. Han, M. Hupalo, D. Appy, H.-Q. Lin, *Prog. Surf. Sci.* **2015**, *90*, 397.
[23] J. Kraus, S. Böcklein, R. Reichelt, S. Günther, B. Santos, T. O. Menteş, A. Locatelli, *Carbon* **2013**, *64*, 377.
[24] G. X. Ni, Y. Zheng, S. Bae, H. R. Kim, A. Pachoud, Y. S. Kim, C. L. Tan, D. Im, J. H. Ahn, B. H. Hong, B. Özyilmaz, *ACS Nano* **2012**, *6*, 1158.
[25] J. S. Alden, A. W. Tsen, P. Y. Huang, R. Hovden, L. Brown, J. Park, D. A. Muller, P. L. McEuen, *Proc. Natl. Acad. Sci. USA* **2013**, *110*, 11256.
[26] L. Brown, R. Hovden, P. Huang, M. Wojcik, D. A. Muller, J. Park, *Nano Lett.* **2012**, *12*, 1609.
[27] T. A. de Jong, E. E. Krasovskii, C. Ott, R. M. Tromp, S. J. van der Molen, J. Jobst, *Phys. Rev. Mater.* **2018**, *2*, 104005.
[28] H. Hibino, H. Kageshima, F. Maeda, M. Nagase, Y. Kobayashi, H. Yamaguchi, *Phys. Rev. B* **2008**, *77*, 075413.
[29] N. Srivastava, Q. Gao, M. Widom, R. M. Feenstra, S. Nie, K. F. McCarty, I. V. Vlassiouk, *Phys. Rev. B: Condens. Matter Mater. Phys.* **2013**, *87*, 245414.
[30] D. P. Gopalan, P. C. Mende, S. C. De La Barrera, S. Dhingra, J. Li, K. Zhang, N. A. Simonson, J. A. Robinson, N. Lu, Q. Wang, M. J. Kim, B. D'Urso, R. M. Feenstra, *J. Mater. Res.* **2016**, *31*, 945.
[31] W. X. Tang, K. L. Man, H. Huang, C. H. Woo, M. S. Altman, *J. Vac. Sci. Technol., B: Microelectron. Nanometer Struct.* **2002**, *20*, 2492.
[32] T. Seyller, R. D. Diehl, *J. Vac. Sci. Technol., A* **1999**, *17*, 1635.
[33] R. M. Feenstra, N. Srivastava, Q. Gao, M. Widom, B. Diaconescu, T. Ohta, G. L. Kellogg, J. T. Robinson, I. V. Vlassiouk, *Phys. Rev. B: Condens. Matter Mater. Phys.* **2013**, *87*, 041406(R).
[34] S. Forti, U. Starke, *J. Phys. D: Appl. Phys.* **2014**, *47*, 094013.
[35] J. Jobst, J. Kautz, D. Geelen, R. M. Tromp, S. J. van der Molen, *Nat. Commun.* **2015**, *6*, 8926.
[36] V. Miseikis, D. Convertino, N. Mishra, M. Gemmi, T. Mashoff, S. Heun, N. Haghighian, F. Bisio, M. Canepa, V. Piazza, C. Coletti, *2D Mater.* **2015**, *2*, 014006.
[37] C. Bouhafs, S. Pezzini, N. Mishra, V. Mišeikis, Y. Niu, C. Struzzi, A. A. Zakharov, S. Forti, C. Coletti, arXiv:2006.06667v1 **2020**.

© 2021 The Authors. Advanced Materials Interfaces published by Wiley-VCH GmbH